Report 49

Petri Räisänen, Markku Rummukainen
and Jouni Räisänen

Modification of the HIRLAM Radiation Scheme for Use in the Rossby Centre Regional Atmospheric Climate Model

Department of Meteorology
UNIVERSITY OF HELSINKI

Department of Meteorology
University of Helsinki
Report No. 49

Modification of the HIRLAM radiation scheme for use in the Rossby Centre regional Atmospheric climate model

by

Petri Räisänen, Markku Rummukainen and Jouni Räisänen

Helsinki 2000

Helsingin yliopisto
Meteorologian laitos

Department of Meteorology
P.O.Box 4 (Yliopistonkatu 3)
FIN-00014 University of Helsinki
FINLAND

ISBN 951-45-9430-4
ISSN 0356-6897

Abstract

Modifications have been implemented to the version of the HIRLAM radiation scheme used in the Rossby Centre regional Atmospheric climate model (RCA). Most importantly, the computation of gaseous longwave (LW) emissivities has been revised so that the emissivities for H_2O line absorption, H_2O continuum absorption and CO_2 absorption are considered separately. The revised scheme also includes stratospheric heating due to O_3 shortwave (SW) absorption and eliminates spurious night-time SW heating present in the results of the original version.

The modifications have been tested in stand-alone radiation computations and in a set of 14-month runs with RCA. The major radiative effects are an increase in outgoing LW radiation (on average by 9 Wm^{-2} for the RCA integration domain) and an increase in the net SW flux at the top of the atmosphere (TOA) particularly in summer. The modifications improve significantly the agreement of TOA clear-sky fluxes with Earth Radiation Budget Experiment data in the LW region but not in the SW region. They also helped to bring the OLR difference between doubled and present CO_2 runs closer to that in the ECHAM4 GCM, which provided the boundary forcing used in this climate change experiment.

On the whole, the modifications have a small effect on the simulation of the present climate by RCA. The land-area average two-metre temperature (T2) is ≈ 0.2 °C higher in summer but ≈ 0.05 °C lower in winter. The land-area average T2 difference between doubled and present CO_2 runs is 0.25 °C larger in annual mean when using the revised radiation code, with a larger impact in summer.

Contents

1 Introduction

In the coming decades and centuries, climate changes are expected to occur as a response to anthropogenic changes in the concentrations of radiatively active atmospheric constituents, in particular, CO_2 and other greenhouse gases. At Rossby Centre in the Swedish Metorological and Hydrological Institude (SMHI), efforts are underway to model these climate changes, as a part of the SWECLIM program. The focus is on high-resolution climate modelling in northern Europe, and the primary tool used in this work is the Rossby Centre regional Atmospheric climate model (RCA) (Rummukainen et al. 1998). A distinct limitation of the RCA model, which builds on the High Resolution Limited Are Model (HIRLAM) version 2.5 (Källen 1996), is, however, that the radiation scheme used (Savijärvi 1990; Sass et al. 1994) includes the effect of atmospheric CO_2 only through predetermined constant correction terms. Thus, the radiative forcing due to changes in CO_2 concentration cannot be modelled. While the effects of this restriction on the model-simulated climate change may be largely alleviated by the fact that RCA "feels" the changes in CO_2 concentration through its lateral boundary conditions and sea surface and deep soil temperatures taken from the driving GCM, it is not obvious that these effects are negligible.

It is the above considerations that gave a motivation to modify the radiation scheme in RCA. The primary modifications include an explicit computation of the effects of CO_2 in the longwave (LW, thermal) region and a revised treatment of water vapor absorption in the LW region and of ozone absorption in the shortwave (SW; solar) region.

When developing the modifications, the ECMWF radiation scheme (Morcrette 1989, 1991) was used as the primary reference. The key features of this scheme and of the original HIRLAM radiation scheme (Sass et al. 1994) are first discussed in section 2. Section 3 describes the modifications implemented to the HIRLAM radiation scheme for use in RCA. Off-line radiation tests, including both standard single-column experiments and extensive tests with GCM-generated data, are described in sections 4 and 5. The results of a set of test runs with RCA addressing the effect of the modifications on the simulation of the present climate and climatic changes are reported in section 6. The report ends with a summary and some concluding remarks in sections 7 and 8.

2 HIRLAM and ECMWF radiation schemes: some description

Apart from the two minor exceptions mentioned in section 3.3, the modifications made to the HIRLAM radiation scheme concern solely the parameterization of clear-air radiative transfer. Therefore, it is sufficient to consider here the treatment of radiation in cloud-free conditions. Information on the treatment of clouds in the HIRLAM and ECMWF radiation schemes can be found in Sass et al. (1994) and Morcrette (1989, 1991), respectively. Furthermore, the modifications mainly concern longwave computations, so the emphasis here is on the treatment of LW radiation.

2.1 HIRLAM scheme

The clear-sky part of the HIRLAM radiation scheme originates from Savijärvi (1990). The LW computations are based on an empirical emissivity function for water vapor line absorption:

$$\epsilon_{\mathrm{H_2O}}(p_i, p_j) = 0.60 + 0.17X - 0.0082X^2 - 0.0045X^3, \tag{1}$$

where

$$X = \log_{10} u(p_i, p_j), \tag{2}$$

and $u(p_i, p_j)$ is the linearly pressure-scaled water vapour path length (in gcm^{-2}) between pressure levels p_i and p_j defined by

$$u(p_i, p_j) = \frac{1}{g} \int_{p_i}^{p_j} q \frac{p}{p_0} dp. \tag{3}$$

Here, $p_0 = 1013$ hPa is a reference pressure, q is the specific humidity (in kg/kg) and g is the gravitational acceleration. The downward LW flux at the surface is computed as

$$F^{\downarrow}_{\mathrm{LW,sfc}} = \int_{p_s}^{0} B(T_p) d\epsilon_{\mathrm{H_2O}}(p, p_s) + 3000 q_N + 35, \tag{4}$$

where $F^{\downarrow}_{\mathrm{LW,sfc}}$ is given in Wm^{-2}, $B(T_p)$ is the Planck function for blackbody radiation at temperature T_p, p_s is the surface pressure, and q_N is the specific humidity in the lower-

most model layer. The first term represents the effect of water vapour line absorption and the second is a crude estimate for the contribution by water vapour continuum absorption. The last term represents nominally the effect of other atmospheric gases (CO_2, O_3, CH_4, N_2O, the CFCs) and aerosols, although it could also be viewed as a tuning factor (indeed, the original value proposed by Savijärvi (1990) was only 16 Wm^{-2}).

The heating or cooling induced by LW radiation is computed from

$$\left(\frac{\partial T_p}{\partial t}\right)_{\mathrm{LW}} = -B(T_p)\frac{g}{C_p}\frac{\partial \epsilon_{\mathrm{H_2O}}(0,p)}{\partial p} + [B(T_s) - B(T_p)]\frac{g}{C_p}\frac{\partial \epsilon_{\mathrm{H_2O}}(p,p_s)}{\partial p} - 11.5q^3 - 2.3 \times 10^{-6}, \quad (5)$$

where the unit of $\left(\frac{\partial T_p}{\partial t}\right)_{\mathrm{LW}}$ is Ks^{-1}, and C_p is the specific heat capacity of air at constant pressure. The first two terms represent the effect of water vapour line absorption, the first being the "cooling-to-space" term and the second the contribution (usually warming) due to energy exchange with the surface. The third term is a crude representation of the effect of water vapour continuum, and the last term is a correction for other gases and aerosols (it could also be regarded as a tuning factor).

The main simplifications in HIRLAM clear-sky longwave calculations are thus as follows:

- The whole longwave region is treated as a single spectral interval.

- Only the effect of H_2O line absorption is computed "properly". For H_2O continuum absorption, ad-hoc parameterizations are used, and other gases and aerosols are lumped into constant correction factors.

- In computing clear-air radiative heating or cooling rates, the energy exchange between atmospheric layers is neglected (this is known as the Sasamori approximation after Sasamori (1972)). To include that, the term

$$\left(\frac{\partial T_p}{\partial t}\right)_{\mathrm{LW,exch}} = \frac{g}{C_p}\int_0^{p_s}[B(T'_p) - B(T_p)]\frac{\partial^2 \epsilon(p,p')}{\partial p \partial p'}dp' \quad (6)$$

  should be added to Eq. (5). Obviously, the evaluation of (6) at each pressure level p would necessitate an integration over all other layers, thereby substantially increasing the computational costs.

The clear-sky downward shortwave flux at the surface is computed in the HIRLAM scheme as

$$\begin{aligned} F^{\downarrow}_{\mathrm{SW,sfc}} &= S\mu_0 \left\{1 - 0.024\mu_0^{-0.5} - a_1 0.11 u_s(p_s)^{0.25} \right. \\ &\quad \left. - a_2 p_s/p_{00} \left[0.28/(1 + 6.43\mu_0) - 0.07\alpha\right]\right\}, \end{aligned} \tag{7}$$

where S is the top-of-the-atmosphere (TOA) solar flux, μ_0 is the cosine of the solar zenith angle θ_0 ($\mu_0 = \cos\theta_0$), p_s is the surface pressure, $p_{00} = 1000$ hPa is a reference pressure, and α is the surface albedo. The pressure-scaled slant water vapour path is

$$u_s(p) = u(0,p)/\mu_0. \tag{8}$$

The first term in Eq. (7) represents the effect of O_3 absorption for a typical total ozone column of 350 DU. The second term represents water vapour absorption; it also includes implicitly the minor effects of O_2 and CO_2 absorption. The last term including two contributions describes the effect of molecular Rayleigh scattering. The coefficients $a_1 = 1.2$ and a_2=1.25 are a crude parameterization for the average effects of aerosol absorption and scattering, respectively.

The clear-sky shortwave heating rate is computed as

$$\left(\frac{\partial T_p}{\partial t}\right)_{\mathrm{SW}} = S\frac{g}{C_p}\frac{p}{p_0}\left[Y(u_s) + 1.67\alpha\mu_0 Y(u_*)\right] + 1.7\times 10^{-6}\mu_0^{0.3}. \tag{9}$$

The two terms in brackets represent water vapour absorption of the direct solar beam and of the beams reflected by the surface, respectively. They are described in more detail in Savijärvi (1990) and Sass et al. (1994). The last term is a parameterization for the absorption by CO_2, O_2 and tropospheric O_3. It does not, however, account for the strong SW heating caused by O_3 absorption in the stratosphere.

2.2 ECMWF scheme

The cycle 45 version of the ECMWF radiation code (from year 1993) was used as the primary reference when modifying the HIRLAM scheme. In many respects, it can be regarded as a typical example of radiation codes used in atmospheric general circulation models. The most salient features of the clear-sky computations include the following:

The longwave region is divided into six spectral intervals. Seven absorbing gases — H_2O, CO_2, O_3, CH_4, N_2O, CFC-11 and CFC-12 — are considered, each being

treated separately; aerosol absorption is also included. Water vapour absorption is further divided into line absorption, foreign-broadened (p-type) continuum and self-broadened (e-type) continuum; the latter is based on Roberts et al. (1976). Otherwise, the gas absorption parameterizations both in the longwave and in the shortwave are based on absorption coefficients fitted from the Air Force Geophysical Laboratory 1982 compilation of line parameters.

In the longwave, the radiative transfer equation is solved using the emissivity-type (i.e., non-scattering) approach. The upward and downward fluxes are evaluated at all model half-levels (layer boundaries), and the LW heating or cooling rate of each layer is computed from the convergence of the net (downward−upward) flux. The energy exchange between different layers is fully accounted for.

The shortwave region is divided into only two spectral intervals, one for the ultraviolet and visible region (0.25–0.68 μm) and one for the near-infrared region (0.68–4.00 μm). Absorption by H_2O and O_3 is treated separately, whereas the less important so-called "uniformly mixed gases" O_2, CO_2, CH_4, N_2O and CO are handled as a single hybrid gas. Molecular scattering is also included, and so is scattering and absorption by five standard aerosol types. The shortwave fluxes at each half-level are determined using the two-stream approach. First, the reflectivities and transmissivities of individual layers are determined; then, the adding method is applied to compute the fluxes as described by Fouquart and Bonnel (1980).

It needs to be stressed that even though the ECMWF radiation scheme is substantially more comprehensive than the HIRLAM scheme, it can by no means considered as an absolute reference. Strictly speaking, no radiation scheme, not even the most rigorous line-by-line (LBL) models, can be given that attribute (Ellingson et al. 1991), due to the uncertainties remaining e.g. in water vapour continuum absorption in the LW. In fact, the ECMWF scheme features some known biases. For example, it underestimates the sensitivity of net LW fluxes to a doubling of atmospheric CO_2 concentration by $\sim 20\%$. Furthermore, it likely overestimates the clear-sky outgoing LW radiation by $\gtrsim 5$ Wm^{-2} (see section 4 for more discussion).

3 Modifications of the HIRLAM scheme

The major modifications implemented to the HIRLAM radiation scheme were a change of computation of gaseous LW emissivities (section 3.1) and the addition of SW heating due to stratospheric ozone (section 3.2). Some other (mainly minor) modifications were also made; these are listed in section 3.3.

3.1 Modification of longwave emissivities

The water vapour emissivity ϵ_{H_2O} in Equations (4) and (5) was replaced by a total gaseous emissivity ϵ_{tot}, including the effects of both H_2O and CO_2. To accomplish this, it was necessary to modify the computation of the water vapour emissivity ϵ_{H_2O}. In the revised formulation, emissivities for H_2O line absorption ϵ_{line} and e-type continuum absorption ϵ_{cont} are considered separately. The effect of p-type continuum is included into ϵ_{line}. The total water vapour emissivity is defined as

$$\epsilon_{H_2O} = \epsilon_{line} + a(1 - \epsilon_{line})\epsilon_{cont}, \tag{10}$$

and the total gaseous emissivity as

$$\epsilon_{tot} = \epsilon_{H_2O} + b(1 - \epsilon_{H_2O})\epsilon_{CO_2}. \tag{11}$$

Here, a and b are "non-overlap" factors between H_2O line absorption and e-type continuum absorption, and between H_2O and CO_2 absorption, respectively.

The determination of an optimal formulation for the terms in Equations (10) and (11) is not a trivial matter. When testing the different formulations, a longwave scheme grossly simplified from the ECMWF scheme was used as an aid. This scheme retains the same vertical integration method as the ECMWF scheme, and thus includes fully the energy exchange between atmospheric layers, but it treats the LW region as a single interval. The scheme, hereafter denoted as ECHIR, is a modified version of that considered by Savijärvi and Räisänen (1998).

In the case of a homogeneous (isothermal and isobaric) optical path, the emissivity for a single absorbing gas is defined as

$$\epsilon(p, T, u) = \frac{\int_0^\infty B_\lambda(T)\left\{1 - \exp\left[-k_\lambda(p, T)u\right] d\lambda\right\}}{\int_0^\infty B_\lambda(T) d\lambda}, \tag{12}$$

where p is the pressure, T is the temperature, u is path length (absorber amount per unit area, e.g. in gcm^{-2}), λ is the wavelength, B_λ is the Planck function, and k_λ is the spectral mass absorption coefficient. Thus the emissivity depends not only on the path length u but also on pressure and temperature because (1) the absorption coefficients k_λ depend both on p and T due to quantum-mechanical reasons (e.g., Goody and Yung 1989) and (2) the shape of the Planck function B_λ depends on T.

In order to account for the pressure and temperature dependence of k_λ, we apply the scaling approximation in which k_λ is evaluated at a fixed reference pressure and temperature but the actual path length u is replaced by an effective path length u_{eff}. The effective path length between pressure levels p_1 and p_2 is defined separately for H_2O line absorption including p-type continuum (u_l), H_2O e-type continuum absorption (u_e) and CO_2 absorption (u_c):

$$u_l = \int_{p_1}^{p_2} q \frac{p}{p_0 g} dp, \tag{13}$$

$$u_e = \int_{p_1}^{p_2} q \frac{e}{p_0 g} \left[1.0121(290/T)^6\right] dp, \tag{14}$$

$$u_c = \int_{p_1}^{p_2} q_{\mathrm{CO_2}} \frac{p}{p_0 g} (T/240)^3 dp. \tag{15}$$

Here, q and $q_{\mathrm{CO_2}}$ are the specific concentrations of H_2O and CO_2 (in kg/kg), e is the partial pressure of water vapour, $p_0 = 1013$ hPa is a reference pressure, and g is the gravitational acceleration.

No attempt was made to explicitly account for the temperature dependence of emissivities arising from the fact that the shape of the Planck function B_λ changes with changing atmospheric temperature. In the case of water vapour e-type continuum absorption and CO_2 absorption, it proved reasonable to use emissivity curves determined for fixed reference temperatures. For ϵ_{cont}, a high reference temperature of 290 K was chosen, consistent with the fact that the effect of e-type continuum increases strongly with increasing specific humidity and, thus, temperature. In the case of CO_2, a reference temperature of 240 K is used, which is more typical of upper tropospheric and stratospheric conditions.

For H_2O line absorption, however, the isothermal emissivity formulation (12) was found to be unsatisfactory. In the case of realistic non-isothermal atmospheres, emissivity curves defined for fixed reference temperatures T_r worked rather poorly for all reas-

onable values of T_r. A more empirical approach was therefore adopted: computations were made for a global GCM-generated data set (see section 5) both with the ECMWF scheme and the ECHIR scheme so that only the absorption by H_2O lines and p-type continuum was accounted for. The coefficients appearing in the emissivity curve in the ECHIR scheme were then chosen so as to minimize the root-mean-square differences of LW fluxes from the ECMWF scheme. This procedure resulted in the following expresssion:

$$\epsilon_{\text{line}} = 6.54860u_l^{0.5} - 11.9669u_l^{0.625} + 7.82396u_l^{0.75} - 1.79180u_l^{0.875}. \tag{16}$$

Strictly speaking, Eq. (16) is not very accurate. When used in the ECHIR scheme, it typically resulted in an underestimate of the downward flux at the surface and an underestimate of the upward flux at the TOA, with average deviations of $\approx 6-7$ Wm^{-2} from the ECMWF scheme. We further found that the accuracy could be improved substantially by defining separate emissivity curves for the computation of upward and downward fluxes, but this approach is unfortunately not feasible in the HIRLAM scheme owing to the use of the Sasamori approximation. To improve the accuracy, we adjusted the tunable parameters appearing in Equations (4) and (5) in the HIRLAM scheme.

For H_2O e-type continuum and CO_2 absorption, the following two-part expressions were chosen:

$$\epsilon_{\text{cont}} = \begin{cases} 31.811u_e - 1463.1{u_e}^2, & u_e < 10^{-2.5}\text{gcm}^{-2} \\ -8.2253 \times 10^{-2} + 3.1258{u_e}^{0.5} - 2.1966u_e & \\ -3.6719{u_e}^{1.5} + 4.0475{u_e}^2, & u_e \geq 10^{-2.5}\text{gcm}^{-2} \end{cases} \tag{17}$$

and

$$\epsilon_{\text{CO}_2} = \begin{cases} 4.5297u_c^{0.5} - 109.83u_c + 1264.4{u_c}^{1.5} & u_c < 10^{-3}\text{gcm}^{-2} \\ 0.21332 + 2.8000 \times 10^{-2} \ln u_c & \\ +2.2341 \times 10^{-3} \ln^2 u_c + 1.6113 \times 10^{-4} \ln^3 u_c & u_c \geq 10^{-3}\text{gcm}^{-2} \end{cases} \tag{18}$$

Note that while the path lengths defined by Equations (13)–(15) are valid for vertical paths, Eqs. (16)–(18) include implicitly the effect of angular integration, which is parameterized in the ECMWF scheme by using the ordinary diffusivity factor of 1.66. These formulae are thus parameterization equations for flux (as opposed to beam)

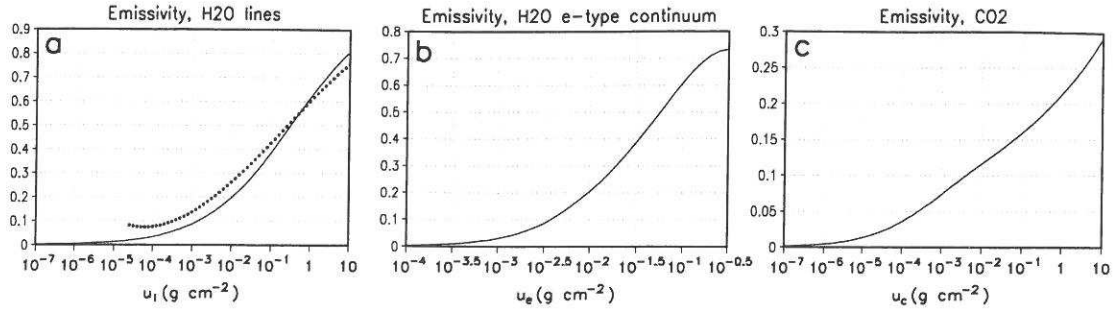

Figure 1 *The emissivity curves in the modified HIRLAM scheme for (a) H_2O line absorption ($\epsilon_{\rm line}$), (b) H_2O e-type continuum absorption ($\epsilon_{\rm cont}$), and (c) CO_2 absorption (ϵ_{CO_2}). Figure 1a also shows the H_2O emissivity curve used in the original HIRLAM scheme [with dots; the values below a minimum path length assumed in the original version ($u_l = 2 \times 10^{-5}$ gcm^{-2}) are omitted.] The largest path lengths considered in this figure represent approximately the limit of validity of the new emissivity curves.*

emissivities.

The emissivity curves defined by Equations (16)–(18) are visualised in Figure 1. Also shown in Fig. 1a is the original emissivity curve (1). In order to put the effective path lengths into a perspective, we note that for the McClatchey et al. (1971) midlatitude summer atmosphere, the H_2O path length u_l for the whole column is 2.4 $\rm gcm^{-2}$, and that above 700 / 300 / 100 hPa is 0.31 / 2.4×10^{-3} / 2.0×10^{-5} $\rm gcm^{-2}$. The respective figures for the e-type path length u_e are 3.0×10^{-2} / 1.6×10^{-3} / 1.7×10^{-6} / 7.2×10^{-10} $\rm gcm^{-2}$, and the corresponding CO_2 path lengths for a CO_2 concentration of 353 ppmv are $u_c = 0.41$ / 0.16 / 2.0×10^{-2} / 2.0×10^{-3} $\rm gcm^{-2}$.

The purpose of the "non-overlap" factors a and b is to account for the spectral correlation there is between H_2O line absorption (including p-type continuum) and e-type continuum absorption and between H_2O and CO_2 absorption, respectively. For example, $b < 1$ ($b > 1$) means that the spectral correlation between H_2O and CO_2 absorption is positive (negative), that is, CO_2 absorption is stronger (weaker) than average in spectral regions where H_2O absorption is stronger than average, and vice versa. As a rule, radiation schemes used in atmospheric GCMs, including the ECMWF scheme, assume that the absorption by different gases is spectrally uncorrelated in each interval considered. This so-called multiplicativity assumption, which is equal to setting $a = b = 1$ in Equations (10) and (11), is feasible when the LW region is divided into several spectral intervals, but not when it is handled as a single entity as in the HIRLAM scheme.

When producing parameterization equations for a and b, use was again made of the GCM-generated data set. This made it possible to choose the most relevant combinations of path lengths u_l, u_e and u_c for consideration, and therefore, to implicitly account for the correlations that exist between them. In broad terms, u_l has a strong positive correlation with u_e, and a weaker but still positive correlation with u_c. Finally, a was parameterized as a function of u_l according to

$$a = 1 + 1.8062u_l^{0.25} - 8.0828u_l^{0.5} + 10.029u_l^{0.75} - 4.948u_l + 0.88512u_l^{1.25}, \tag{19}$$

and b was parameterized in terms of both u_l and the carbon dioxide concentration c_{CO_2} (in ppmv):

$$\begin{aligned} b \;=\; & 1 + 0.11293u_l^{0.25} + (4.478 + 1.4774 \times 10^{-2}X)u_l^{0.5} \\ & -(9.777 + 8.5438 \times 10^{-2}X)u_l^{0.75} + (6.313 + 0.19318X)u_l \\ & -(1.317 + 8.1497 \times 10^{-2}X)u_l^{1.25} \end{aligned} \tag{20}$$

where

$$X = 2.1449\left[(c_{CO_2}/500)^{1/3} - 1\right]. \tag{21}$$

The above parameterization equations are visualized in Figure 2. It can be seen that when $u_l \to 0$, both a and $b \to 1$. This is what necessarily happens in the "non-overlap" factor formulation when H_2O line absorption is weak throughout the spectrum, so there are no significant overlap effects. When u_l increases, a first attains values slightly larger than 1 but then decreases to below 0.7 (for $u_l \approx 0.5$ gcm^{-2}), and increases again at very large values of u_l (and, thus, of u_e). It is possible to trace this somewhat complicated behaviour to the facts that (1) H_2O line absorption occurs throughout the spectrum, being strongest in the central parts of the rotation band (wavenumber $\nu < 350$ cm^{-1}) and in the vibration-rotation band (1450–1880 cm^{-1}) and weakest in the atmospheric window (800–1250 cm^{-1}); and (2) that H_2O $e-$type continuum is included in the ECMWF scheme between 350 and 1250 cm^{-1}, with strength decreasing with increasing wavenumber.

On the other hand, CO_2 absorption mainly occurs in the 15 μm band, with much weaker bands in the window region. At relatively small values of u_l, $b > 1$ with a maximum of over 1.3 at $u_l \approx 0.07$ gcm^{-2}, because the parts of the H_2O rotation band overlapping the CO_2 15 μm band are still quite transparent. With increasing u_l,

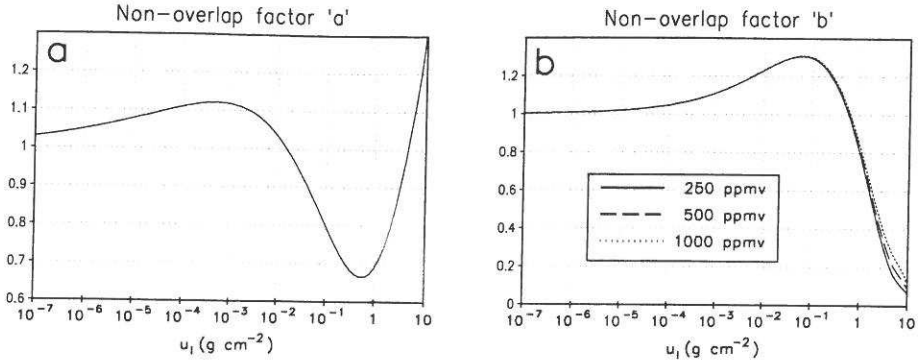

Figure 2 *(a) The "non-overlap" factor between (a) H_2O line absorption and e-type continuum absorption, and (b) between H_2O and CO_2 absorption for three different CO_2 concentrations.*

also these weaker parts of the rotation band start to saturate, and therefore b drops to values substantially below 1. The increase of the values of b with increasing CO_2 concentration, which is apparent for large values of u_l, occurs because the relative contribution to ϵ_{CO_2} of the weak CO_2 bands in the atmospheric window increases with increasing CO_2 path length u_c.

3.2 Ozone shortwave absorption

The original version of the HIRLAM radiation scheme accounts for the depletion of the downward SW flux at the surface $F^{\downarrow}_{\mathrm{SW,sfc}}$ caused by O_3 absorption; however, it does not include the strong stratospheric heating caused by it. This is somewhat illogical, and moreover, the problem is accentuated by the inclusion of CO_2 LW effects in the modified scheme. Stratospheric LW cooling is much stronger than for the original scheme (see Figure 5), which could lead to a cold bias in the stratosphere if not compensated by some other process. In the global mean, the stratosphere is close to radiative equilibrium, O_3 SW absorption being by far the most important mechanism balancing the LW cooling caused predominantly by CO_2 (e.g., Manabe and Strickler 1964; Mlynczak et al. 1999).

To include the SW heating due to O_3 absorption, a crude but computationally very efficient approach was chosen. A precomputed heating term $\left(\frac{\partial T}{\partial t}\right)_{O_3}$ is added to clear-sky SW heating, defined so that its vertical integral (ABS_{O_3}) equals the reduction of

$F^{\downarrow}_{\mathrm{SW,sfc}}$ caused by O_3 absorption (assuming a total ozone column of 350 DU):

$$\mathrm{ABS}_{O_3} = \int_0^{p_s} \frac{C_p}{g} \left(\frac{\partial T}{\partial t}\right)_{O_3} dp = 0.024 S \mu_0^{0.5} \tag{22}$$

For simplicity, the O_3 absorption of reflected beams is neglected, which actually leads to a slight underestimate of ABS_{O_3}. The vertical distribution of the heating is defined by

$$\left(\frac{\partial T}{\partial t}\right)_{O_3} = \frac{g}{C_p p_s} \mathrm{ABS}_{O_3} \frac{df_{O_3}}{d\eta}, \tag{23}$$

where f_{O_3} is the cumulative normalized O_3 absorption from the TOA downwards, and η is the hybrid vertical coordinate used in RCA. [1] Based on calculations made with the ECMWF scheme for the McClatchey et al. (1971) standard atmospheres, the following formulation was chosen for f_{O_3}:

$$f_{O_3} = 1 - \exp\left[-6.52978 \times 10^{-3} X - 0.178512 X^2 + 7.13869 \times 10^{-2} X^3 \right. \\ \left. -1.45003 \times 10^{-2} X^4 + 7.36790 \times 10^{-4} X^5\right], \tag{24}$$

where

$$X = \ln(1 + 1000\eta). \tag{25}$$

Figure 3 shows the vertical distribution of O_3 absorption resulting from Equations (22)–(25). It can be seen that the radiative heating due to O_3 absorption peaks near the stratopause and that half of it occurs above $\approx$ 20 hPa.

3.3 Other modifications

The following modifications were also implemented to the radiation scheme:

- In the computation of $F^{\downarrow}_{\mathrm{LW,sfc}}$ [Eq. (4)], the additional term $c_{\mathrm{sur1}} = 35$ Wm^{-2} was reduced to 15 Wm^{-2}. This includes the average contributions by O_3, CH_4, N_2O, CFCs and aerosols (for present concentrations), plus some tuning to compensate for the underestimate of $F^{\downarrow}_{\mathrm{LW,sfc}}$ caused by the use of (16) for H_2O line absorption and a likely low bias in $F^{\downarrow}_{\mathrm{LW,sfc}}$ in the ECMWF scheme.

- The additional term $c_{\mathrm{add}} = -2.3 \times 10^{-6}$ Ks^{-1} (≈ -0.2 Kd^{-1}) in Eq. (5) is now defined as a function of altitude: $c_{\mathrm{add}} = -1.5 \times 10^{-6}$ Ks$^{-1}(3\eta - 1)$. The magnitude

[1] In practise, η(p) differs fairly little from σ(p) $= p/p_s$; for $p_s = 1000$ hPa $\eta = \sigma$ for all p.

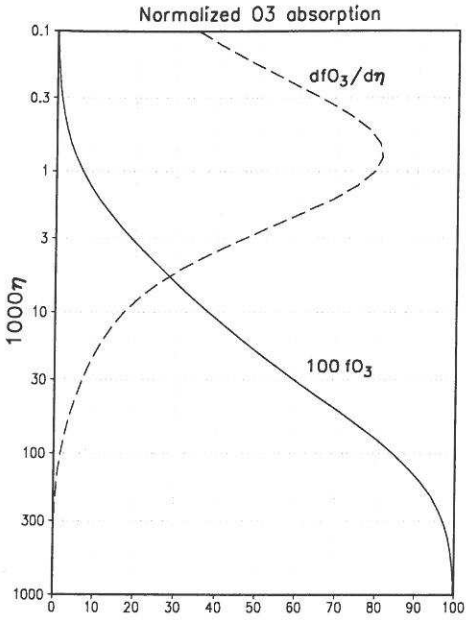

Figure 3 *Normalized vertical distribution of O_3 absorption in the modified HIRLAM scheme. Solid line (fO_3 multiplied by 100) — cumulative absorption from the TOA downwards; dashed line ($dfO_3/d\eta$) — local radiative heating. For $\mu_0 = 0.5$, $dfO_3/d\eta = 1$ corresponds to a heating rate of $\approx 0.2\ Kd^{-1}$.*

of c_{add} was adjusted so as to tune the outgoing LW radiation, and its form was chosen so as to slightly reduce the heating rate differences from the ECMWF scheme.

- The ad-hoc correction terms for water vapour continuum in Equations (4) and (5) are, of course, neglected in the modified scheme. The revised equations for $F^{\downarrow}_{\text{LW,sfc}}$ and $\left(\frac{\partial T}{\partial t}\right)_{\text{LW}}$ thus read:

$$F^{\downarrow}_{\text{LW,sfc}} = \int_{p_s}^{0} B(T_p) d\epsilon_{\text{tot}}(p, p_s) + 15, \tag{26}$$

$$\begin{aligned}\left(\frac{\partial T_p}{\partial t}\right)_{\text{LW}} &= -B(T_p)\frac{g}{C_p}\frac{\partial \epsilon_{\text{tot}}(0,p)}{\partial p} + [B(T_s) - B(T_p)]\frac{g}{C_p}\frac{\partial \epsilon_{\text{tot}}(p,p_s)}{\partial p} \\ &\quad -1.5 \times 10^{-6}(3\eta - 1).\end{aligned} \tag{27}$$

- In the original version, radiative heating (both LW and SW) is set to zero above $\eta = 0.05$ ($\approx$ 50 hPa). This is no longer done in the modified scheme, which includes a more proper treatment of the radiative processes of importance in the stratosphere.

- The computation of the "heating-from-ground" term in the lowest model layer has been modified. This term is proportional to the difference between the surface temperature and the effective radiation temperature of the lowest layer for downward radiation ($T_s - T_{\rm eff}^{\downarrow}$). Originally, the temperature at the lowest model full-level was used for $T_{\rm eff}^{\downarrow}$. In reality, however, the major part of the LW radiation coming to the surface from the lowest model layer is emitted within the lower half of that layer, and therefore, the difference $T_s - T_{\rm eff}^{\downarrow}$ should be reduced. Semi-empirically, it is multiplied by 2/3 in the revised version.

- Two other minor modifications were also implemented to the LW calculations. Physically, they are modifications of clear-air radiative transfer, but they affect the results only in the presence of clouds. First, the single-layer clear-air emissivity, appearing in the definition of the empirical function G_j in Sass et al. (1994), is now computed as

$$\epsilon = \epsilon_{\rm line} + 0.12, \tag{28}$$

the latter term being the typical contribution by H_2O e-type continuum and CO_2 absorption. Second, the term $a_9 - f_3$ in Equation (25) of Sass et al. (1994) is now replaced by 15η (in Wm^{-2}). Physically, this corresponds to the assumption that the "extra" term of the clear-sky downward LW flux increases linearly with pressure from 0 at the TOA to 15 Wm^{-2} at the surface.

- An empirical solar zenith angle correction of the surface albedo

$$\alpha(\mu_0) = \overline{\alpha} + \frac{0.2}{1 + \mu_0} - 0.10, \tag{29}$$

where $\overline{\alpha}$ is the "climatological" albedo and μ_0 is the cosine of the solar zenith angle, was modified by increasing the last term to 0.12. This avoids a systematic increase of surface albedo caused by the above correction in its original form. Note that this modification was implemented already in the early phase of this work (December 1998) and that it is included in the off-line and on-line tests with the "original" radiation scheme reported below.

- Lastly, a fairly important bug correction was made to the SW calculations. For convenience, a minimum value 0.01 is used for μ_0 in the scheme; in the original version this is done also in areas where the sun is really below the horizon, which leads to non-zero SW heating at night. In the revised version, the SW results are set to zero when the real $\mu_0 < 0$, which reduces the average atmospheric SW absorption by ~ 6 Wm^{-2}.

3.4 Computer time requirements

Tests made with Cray C94 (Centre for Scientific Computing, Finland) indicated that the revised version of the HIRLAM radiation scheme needs $\approx 25\%$ more CPU time than the original version (for a vector length of 100, including full optimization but no parallelization).

4 Single-column experiments

As the first validation exercise, we consider the performance of the HIRLAM radiation scheme in single-column test cases defined in the Intercomparison of Radiation Codes in Climate Models (ICRCCM) project (Ellingson et al. 1991; Fouquart et al. 1991).

4.1 Longwave test cases

Table 1 shows the results obtained with the original and modified version of the HIRLAM scheme in selected ICRCCM longwave test cases. These results were computed in a 19-layer vertical grid (the HADCM2 vertical grid used in the first long simulations with RCA (Rummukainen et al. 1998)). Note that although the HIRLAM scheme is designed to compute the radiative fluxes only at the surface, the net flux at each level can be inferred by vertically integrating the radiative heating rate:

$$F^{\mathrm{net}}(p) \equiv F^{\downarrow}(p) - F^{\uparrow}(p) = F^{\mathrm{net}}(p_s) - \int_{p_s}^{p} \frac{C_p}{g} \left(\frac{\partial T}{\partial t} \right) dp \qquad (30)$$

Several other results are provided in Table 1 for comparison. The results for the ECMWF scheme and for the Rapid Radiative Transfer Model (RRTM) of Mlawer et al. (1997) were computed by the first author of this report. The RRTM might actually be

8 Concluding remarks

Even though the impact of the radiation scheme modifications appears, in most respects, either positive or neutral, there are several aspects of the present work that could be criticised. For one thing, the ECMWF cycle 45 radiation code might not have been the ideal choice for the scheme used as reference when modifying the RCA radiation scheme. In principle, for example the RRTM (Mlawer et al. 1997) scheme might have been a better alternative, since it includes a probably more accurate water vapour continuum (Clough et al. 1992) and its response to changes in CO_2 concentration is very close to that of line-by-line models. The newest version of the ECMWF scheme also includes an updated continuum parameterization (Zhong and Haigh 1995). Second, we have mainly concentrated on LW clear-sky computations, even though there is likely room for improvement also in the SW part of the RCA (or HIRLAM) radiation scheme and, in particular, in the treatment of clouds. Third, when validating the modifications, it would be pertinent to perform some comparison to observed radiative fluxes not only at the TOA (as done here) but also at the surface.

A more deep-going question is, however, whether the strategy chosen for parameterization of radiation in RCA is optimal. While in most other regional climate models, the treatment of atmospheric physics, including radiation, is equally comprehensive as in global models (Giorgi and Mearns 1999), a very fast highly parameterized radiation scheme is used in RCA. The advantage of this is that it makes it feasible to perform the radiation computations at every time step, so that radiative fluxes and heating rates respond without delay to changes in cloudiness. However, the speed is achieved at the cost of physical simplifications, which inevitably means lower accuracy in some respects. For one thing, the longwave computations are based on the Sasamori approximation, in which the energy exchange between atmospheric layers is neglected. This leads to some biases in LW clear-sky heating rates, and more importantly — because it really is not feasible to totally neglect the energy exchange in the presence of clouds — it necessitates an elaborate approach for the computation of cloud effects. While this approach is fast, its accuracy is limited (see Fig. 6 and the related discussion); furthermore, it appears highly uncertain whether the accuracy could be improved appreciably without rewriting large parts of the code.

A pertinent question is whether the benefits of computing radiative fluxes at every time step are so large for regional climate modelling that they outweigh the increased accuracy (e.g., in the latitudinal distribution of LW cloud forcing) that could be

achieved by using, instead of the present RCA radiation code, a state-of-the-art GCM-type radiation scheme. Such choices should be based on testing.

Even if it proves important to keep the "radiative time step" short, it is not self-evident that the approach taken in RCA is the best possible. On one hand, it may be noted that in more comprehensive radiation schemes like the ECMWF scheme, a very substantial part of the computational time is spent in computing LW gas absorption. Gaseous transmission functions do not change rapidly with time, so one might think of an approach in which the cloud effects are updated at every time step but the gaseous transmissivities are kept fixed for several hours. On the other hand, a new and very promising approach, at least for LW computations, is the use of neural network techniques. Chevallier et al. (1998) have demonstrated that it is possible to teach a neural network to mimick the functioning of a comprehensive longwave scheme with little loss in accuracy but with dramatic savings in computational costs.

Acknowledgements

Drs. Markku Rummukainen and Jouni Räisänen work at the Rossby Centre in the Swedish Meteorological and Hydrological Institute, Norrköping, Sweden. The ERBE and ISCCP data used in this research were obtained from the NASA Langley Research Center EOSDIS Distributed Active Archive Center.

References

Barkstrom, B., E. Harrison, G. Smith, R. Green, J. Kibler, R. Cess and the ERBE Science Team, 1989: Earth Radiation Budget Experiment (ERBE) archival and April 1985 results. *Bull. Amer. Meteor. Soc.*, **70**, 1254–1271.

Cess, R. D., M. H. Zhang, P. Minnis, L. Corsetti, E. G. Dutton, B. W. Forgan, D. P. Garber, W. L. Gates, J. J. Hack, E. F. Harrison, X. Jing, J. T. Kiehl, C. N. Long, J.-J. Morcrette, G. L. Potter, V. Ramanathan, B. Subasilar, C. H. Whitlock, D. F. Young and Y. Zhou, 1995: Absorption of solar radiation by clouds: Observations versus models. *Science*, **267**, 496–499.

Chevallier, F., F. Cheruy, N. A. Scott and A. Chedin, 1998: A neural network approach for a fast and accurate computation of a longwave radiative budget. *J. Appl. Meteor.*, **37**, 1385–1397.

Chou, M.-D., 1990: Parameterizations for the absorption of solar radiation by O_2 and CO_2 with application to climate studies. *J. Climate*, **3**, 209–217.

Clough, S. A. and M. J. Iacono, 1995: Line-by-line calculation of atmospheric fluxes and cooling rates, 2: Application to carbon dioxide, ozone, methane, nitrous oxide and the halocarbons. *J. Geophys. Res.*, **100**, 16519–16535.

Clough, S. A., M. J. Iacono and J.-L. Moncet, 1992: Line-by-line calculations of atmospheric fluxes and cooling rates: Application to water vapor. *J. Geophys. Res.*, **97**, 15761–15785.

Edwards, J. M. and A. Slingo, 1996: Studies with a flexible new radiation code. I: Choosing a configuration for a large-scale model. *Quart. J. Roy. Meteor. Soc.*, **122**, 689–719.

Ellingson, R. G., J. Ellis and S. Fels, 1991: The intercomparison of radiation codes used in climate models: Longwave results. *J. Geophys. Res.*, **96**, 8929–8953.

Fouquart, Y. and B. Bonnel, 1980: Computations of solar heating of the Earth's atmosphere: A new parameterization. *Contrib. Atmos. Phys.*, **53**, 35–62.

Fouquart, Y., B. Bonnel and V. Ramaswamy, 1991: Intercomparing shortwave radiation codes for climate studies. *J. Geophys. Res.*, **96**, 8955–8968.

Gibson, J. K., P. Kållberg, S. Uppala, A. Hernandez, A. Nomura and E. Serrano, 1997: ERA description. ECMWF Re-Analysis Project Rep. Ser. 1, European Centre for Medium-Range Weather Forecasts, Reading, United Kingdom. 66 pp.

Giorgi, F. and L. O. Mearns, 1999: Introduction to special section: Regional climate modeling revisited. *J. Geophys. Res.*, **104**, 6335–6352.

Goody, R. M. and Y. L. Yung, 1989: *Atmospheric radiation. Theoretical basis.* Oxford University Press. 519 pp.

Kållberg, P., 1997: Aspects of the re-analysed climate. ECMWF Re-Analysis Project Rep. Ser. 2, European Centre for Medium-Range Weather Forecasts, Reading, United Kingdom. 89 pp.

Källen, E., ed., 1996: *HIRLAM documentation manual. System 2.5.* 178 pp. + 55 pp. appendix.

Li, Z., L. Moreau and A. Arking, 1997: On solar energy disposition: A perspective from observation and modelling. *Bull. Amer. Meteor. Soc.*, **78**, 53–70.

Manabe, S. and R. F. Strickler, 1964: Thermal equilibrium of the atmosphere with a convective adjustment. *J. Atmos. Sci.*, **21**, 361–385.

McClatchey, R. A., R. W. Fenn, J. E. A. Selby, F. E. Volz and J. S. Garing, 1971: Optical properties of the atmosphere. Report AFCRL-71-0279, Air Force Cambridge Research Laboratories. 85 pp., available from Air Force Geophysics Laboratory, Hanscom Air Force Base, MA 01731, United States.

Mlawer, E. J., S. J. Taubman, P. D. Brown, M. J. Iacono and S. A. Clough, 1997: Radiative transfer for inhomogeneous atmospheres: RRTM, a validated correlated-k model for the longwave. *J. Geophys. Res.*, **102**, 16663–16682.

Mlynczak, M. G., C. J. Mertens, R. R. Garcia and R. W. Portmann, 1999: A detailed evaluation of the stratospheric heat budget, 2: Global radiation balance and diabatic circulations. *J. Geophys. Res.*, **104**, 6039–6066.

Morcrette, J.-J., 1989: Description of the radiation scheme in the ECMWF model. Technical Memorandum 165, European Centre for Medium Range Weather Forecasts, Research Department, Reading, United Kingdom. 26 pp.

Morcrette, J.-J., 1991: Radiation and cloud radiative properties in the European Centre for Medium Range Weather Forecasts forecasting system. *J. Geophys. Res.*, **96**, 9121–9132.

Omstedt, A. and L. Nyberg, 1996: Response of Baltic Sea ice to seasonal, interannual forcing and climate change. *Tellus*, **48A**, 644–662.

Ramanathan, V., B. Subasilar, G. J. Zhang, W. Conant, R. D. Cess, J. T. Kiehl, H. Grassl and L. Shi, 1995: Warm pool heat budget and shortwave cloud forcing: A missing physics? *Science*, **267**, 499–503.

Rasch, P. J. and J. E. Kristjánsson, 1998: A comparison of the CCM3 model climate using diagnosed and predicted condensate parameterizations. *J. Climate*, **11**, 1587–1614.

Ritter, B. and J.-F. Geleyn, 1992: A comprehensive radiation scheme for numerical weather prediction models with potential applications in climate simulations. *Mon. Wea. Rev.*, **120**, 303–325.

Roberts, R. E., L. M. Biberman and J. E. A. Selby, 1976: Infrared continuum absorption by atmospheric water vapor in the 8–10 μm window. *Applied Optics*, **15**, 2085–2090.

Roeckner, E., L. Bengtsson, J. Feichter, J. Lelieveld and H. Rodhe, 1998: Transient climate change simulations with a coupled atmosphere-ocean GCM including the tropospheric sulfur cycle. Report 266, Max Planck Institute für Meteorologie, Hamburg, Germany. 48 pp.

Rossow, W. B., A. W. Walker, D. E. Beuschel and M. D. Roiter, 1996: International Satellite Cloud Climatology Project ISCCP documentation of new cloud data sets. WMO/TD No. 737, World Meteorological Organization, Geneva, Switzerland. 115 pp.

Rummukainen, M., J. Räisänen, A. Ullerstig, B. Bringfelt, U. Hansson, P. Graham and U. Willen, 1998: RCA — Rossby Centre regional Atmospheric climate model: model description and results from the first multi-year simulation. Reports Meteorology and Climatology 83, SMHI. 76 pp.

Räisänen, J., M. Rummukainen, A. Ullerstig, B. Bringfelt, U. Hansson and U. Willen, 1999: The first Rossby Centre regional climate scenario — dynamical downscaling of CO_2-induced climate change in the HadCM2 GCM. Reports Meteorology and Climatology 85, SMHI. 60 pp.

Räisänen, P., 1998: Effective longwave cloud fraction and maximum-random overlap of clouds: A problem and a solution. *Mon. Wea. Rev.*, **126**, 3336–3340.

Räisänen, P., 1999: Parameterization of water and ice cloud near-infrared single-scattering co-albedo in broadband radiation schemes. *J. Atmos. Sci.*, **56**, 626–641.

Sasamori, T., 1972: A linear harmonic analysis of atmospheric motion with radiative dissipation. *J. Meteor. Soc. Japan*, **50**, 505–517.

Sass, B. H., L. Rontu and P. Räisänen, 1994: HIRLAM-2 radiation scheme: Documentation and tests. HIRLAM Technical Report 16, SMHI. 43 pp.

Savijärvi, H. and P. Räisänen, 1998: Long-wave optical properties of water clouds and rain. *Tellus*, **50A**, 1–11.

Savijärvi, H., 1990: Fast radiation parameterization schemes for mesoscale and short-range forecast models. *J. Appl. Meteor.*, **29**, 437–447.

Schwarzkopf, M. D. and S. B. Fels, 1991: The simplified exchange method revisited: An accurate, rapid method for computation of infrared cooling rates and fluxes. *J. Geophys. Res.*, **96**, 9075–9096.

Tanre, D., J.-F. Geleyn and J. M. Slingo, 1984: First results of the introduction of an advanced aerosol-radiation interaction in the ECMWF low resolution global model. In: *Aerosols and Their Climatic Effects* (edited by Gerber, H. E. and A. Deepak), pp. 133–177. A. Deepak Publishing, Hampton, VA, United States.

Wild, M., A. Ohmura, H. Gilgen, E. Roeckner, M. Giorgetta and J.-J. Morcrette, 1998: The disposition of radiative energy in the global climate system: GCM-calculated versus observational estimates. *Climate Dyn.*, **14**, 853–869.

Wu, M.-L. C., 1980: The exchange of infrared radiative energy in the troposphere. *J. Geophys. Res.*, **85**, 4084–4090.

Zhong, W. and J. D. Haigh, 1995: Improved broadband emissivity parameterization for water vapor cooling rate calculations. *J. Atmos. Sci.*, **52**, 124–138.